# ANALYSIS OF THE INTERLAMINAR CRACK INITIATION IN MIXED-MODE I+II COMPOSITE FRACTURE SPECIMENS

András SZEKRÉNYES* and József UJ**

*Department of Applied Mechanics
Budapest University of Technology and Economics
H–1521 Budapest, Hungary
Phone: +36 1 463 1170
e-mail: szeki@mm.bme.hu
**Department of Applied Mechanics
Budapest University of Technology and Economics
H–1521 Budapest, Hungary
Phone: +36 1 463 2228
e-mail: uj@mm.bme.hu

Received: January 20, 2003

## Abstract

The interlaminar crack initiation in mixed-mode specimens was investigated through two- and three-dimensional finite element models. Elastic analysis was conducted to understand the crack initiation in glass-fibre/vinylester composites. The MMF and CLS specimens were used for the two-dimensional plane strain models. Simplified 3D micro-mechanical models were constructed to investigate the effect of the fibres on the stress distribution based on the square fibre arrangement. The mixed-mode conditions were produced by changing the ratio of the crack opening and crack shearing displacement components. It was concluded that the fibre/matrix interface plays critical role in the direction of the crack propagation path. The propagation path was described by the crack angle determined by the peak stresses in the crack front and in the fibre/matrix interface. The critical fibre/matrix interface stress was also determined and found to increase with the mode-I contribution. The tensile stresses ahead of the crack-tip were examined and experienced as increasing with the mode-I contribution.

*Keywords:* unidirectional composite, crack growth, crack angle, fracture mechanics, fracture toughness.

## 1. Introduction

The interlaminar fracture is one of the primary failure modes in laminated composite materials. The mode-I, mode-II and mixed-mode I+II interlaminar fracture properties are intensively studied by designers in literature. The specimens used in the fracture test have a wide range of application. The main aspect of these specimens is the crack, which ensures the location and progression of the fracture. The fracture has several aspects, which can significantly affect the fracture occurrence and progression as well as the fracture properties of the laminated composites. Numerous papers deal with the experimental investigation of the composite fracture properties. The DCB (double cantilever beam), WIF (wedge-insert flexure) [1] specimens for mode-I, the ENF (end-notched flexure), ELS (end-loaded split) [2, 3] specimens

for mode-II, and finally the SCB (single cantilever beam), MMF (mixed-mode flexure) and CLS (cracked-lap shear) [4, 5] specimens for mixed-mode I+II fracture are established by researchers. The MMF test can be conducted in a special bending fixture, while the CLS test requires tensile loading. Applying these tests the mixed-mode I+II fracture toughness ($G_{I+IIC}$) can be determined. The finite element method is suitable to investigate the fracture properties, such as fracture toughness, stress intensity factor as well as the stress distribution and concentration around the starting defect. The finite element analyses can be carried out to investigate the micro-mechanical stress distribution in the composite. TODO and JAR presented a micro-macro-mechanical finite element study about the interlaminar crack growth in glass fibre/epoxy matrix DCB specimens for mode-I [6]. Specimens with symmetric stacking sequence were used. A thin polypropylene film was placed between the central layers. Two- and three-dimensional analyses were carried out to investigate the stress distribution along the contour of the crack front. The crack was assumed to have an elliptical shape, the bluntness of the crack-tip was varied by changing the aspect ($a_0/b_0$) of the ellipse. As the crack-tip bluntness increases, the point of the maximum principal stress moves from the crack-tip towards the corner, including crack growth towards the fibre/matrix interface. A similar investigation was conducted again by TODO et al. using the mode-II ENF specimen and glass-fibre/vinylester composite [7]. It was concluded, that in mode-II loading the crack progression depends on the fibre/matrix interface properties. A relatively weak interface causes that the crack initiates at the fibre/matrix interface. On the other hand, the crack initiates at the crack-tip in the case of strong fibre/matrix connection. In both studies it was concluded that the bond strength at the fibre/matrix interface plays significant role in determining the mode-I and mode-II interlaminar fracture toughness of the composite measured from the DCB and ENF test, respectively. When the fracture initiated from the fibre/matrix interface instead of at the crack-tip the measured interlaminar fracture toughness would reflect the fibre/matrix interfacial strength. TODO and JAR found, that the crack growth path computed from the FE model corresponded well with the experimentally observed path. It was proved by scanning electron microscopy (SEM) in [6, 7]. The current study assumes that under mixed-mode I+II loading similar conditions exist, and results can be regarded as valid.

Considering delamination problems in practice the composite materials are subjected to the combination of mode-I and mode-II loading, hence the mixed-mode I+II loading relates to more realistic conditions. In this paper the mixed-mode loading and fracture initiation is analyzed by the finite element method and the finite element code COSMOS/M 2.0 was utilized. The MMF and CLS specimens were used for the 2D analysis to investigate the local stress distribution and concentration at the crack front. The same material was used as in [6]. Micromodels were constructed to facilitate the understanding of the role of the fibres in the stress distribution of the surrounding matrix using the square fibre arrangement.

## 2. Finite Element Models

### 2.1. 2D Finite Element Model

*Fig. 1* shows the MMF and CLS specimens as the meshed finite element models and the details of the crack-tip. Four-node PLANE2D elements were used under plane strain condition. Dimensions and boundary conditions are also depicted in *Fig. 1*. The CLS specimen consists of 3904 elements and 4119 nodes, the MMF specimen consists of 3210 elements and 3365 nodes, respectively. The stacking sequence of the specimens is depicted in *Fig. 2*. The starting crack exists along the distance denoted by '*a*', it was placed on the mid-plane, in the insert film. The contact between both sides of the crack was avoided due to the mixed-mode loading. The elastic properties of the composite shown in *Fig. 2* (macromechanical properties):

- stiched $0°/90°$ layer (isotropic): $E = 10$ GPa, $\nu = 0.3$
- resin-rich region: $E = 3.1$ GPa, $\nu = 0.35$
- unidirectional layer: $E_1 = 26.6$ GPa, $E_2 = E_3 = 4.7$ GPa, $G_{12} = G_{13} = G_{23} = 1.7$ GPa, $\nu_{12} = \nu_{13} = \nu_{23} = 0.3$.

Four levels of bluntness were investigated in the 2D models: $a_0 = 0.001$, $a_0 = 0.002$, $a_0 = 0.003$, $a_0 = 0.004$ and $b_0 = 0.004$ was held on constant value.

### 2.2. 3D Finite Element Model

The three-dimensional model is illustrated in *Fig. 3*. The details of the crack-tip in the three-dimensional model are depicted at the bottom of *Fig. 3*. The square fibre arrangement was used, the periodicity in the direction '*y*' was included. Eight-node, linear elastic SOLID elements were utilized for the analysis. The 3D model contains 23040 elements and 25520 nodes. The 3D model was used to investigate the crack growth varying the mode-ratio, according to this the mode-I and mode-II contribution was changed. The other aim was to understand the role of the fibres on the stress distribution in the surrounding matrix. The following elastic material properties were used (micromechanical properties, both the fibre and matrix are isotropic)

- epoxy matrix: $E = 3.1$ GPa, $\nu = 0.35$
- glass-fibre: $E = 69$ GPa, $\nu = 0.22$
- fibre-volume fraction: $V_f = 0.35$

It must be noted, that in the 3D model in mode-I the displacement component of '*w*' (crack opening displacement, COD) was uniformly distributed in the top surface of the model, while the bottom surface was constrained in the normal direction. Although the 2D models produce distinct and more complicated displacement field, the effects of these were neglected. In mode-II the in-plane shear was simulated by moving the lower and upper surfaces in the opposite direction (crack shearing
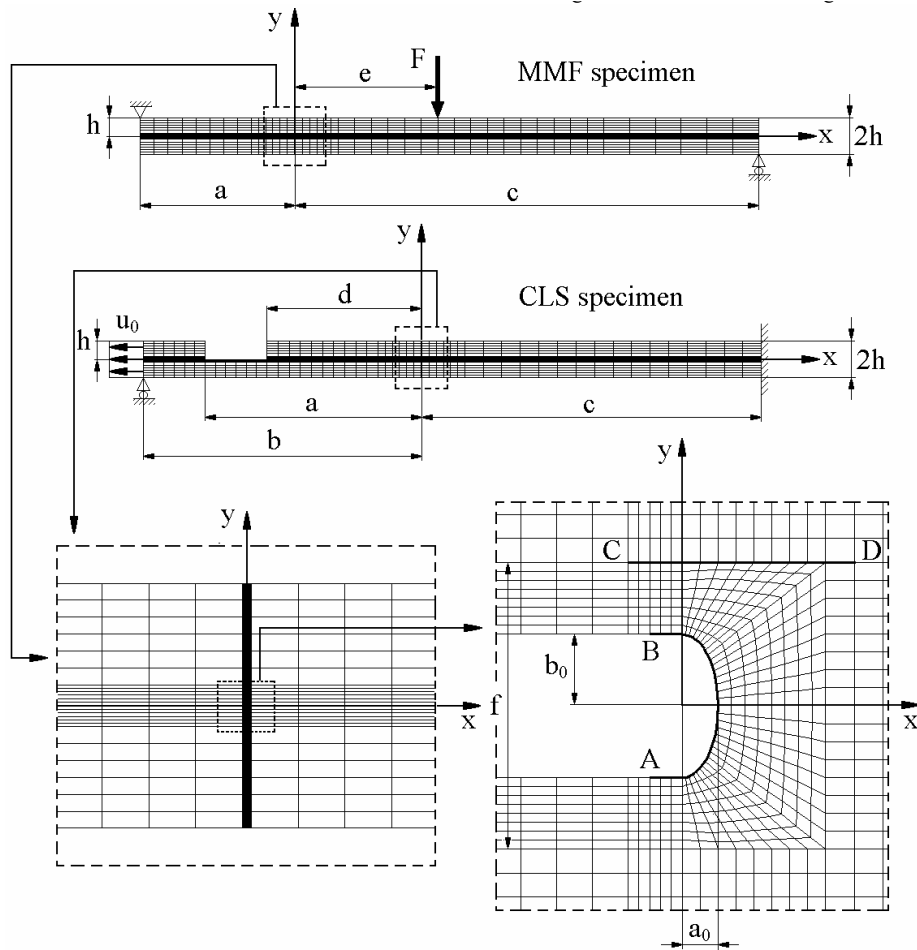
*Fig. 1.* 2D finite element models and details of the crack-tip. MMF specimen: $a = 25$, $c = 75$, $e = 25$, $h = 3$, $f = 0.016$, $F = 1$N. CLS specimen: $a = 35$, $b = 45$, $c = 55$, $d = 25$, $h = 3$, $f = 0.016$, $u_0 = 0.05$, all distances and displacement in [mm]. Line A–B – distance along the crack front, line C–D – distance along the central layer/unidirectional layer interface

displacement, CSD). In mixed-mode I+II loading the ratio of the crack opening and crack shearing displacements was varied. In fact examining the sum of the reaction forces in the upper and lower boundary surfaces the loading measured in [N] can be computed, the mixed-mode conditions could be characterized by the variation of the ratio of the crack opening and shearing forces. However, this problem cannot be handled using forces as loading, the prescription of displacement components is more convenient and accurate. The reaction forces were investigated and found to be having values in the same order comparing the opening and shearing components. The further boundary conditions are shown in *Table 1*. In both models the crack was assumed to have an elliptical shape. The 3D analyses were carried out in the case of $a_0 = 0.002$.
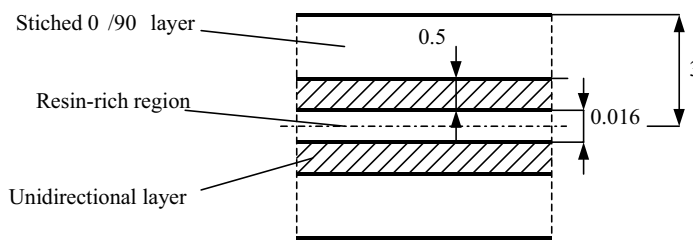


*Fig. 2*. Stacking sequence of the 2D finite element models

*Table 1*. Kinematic boundary conditions for the 3D model

| Boundary surface | Mode-I | Mode-II | Mixed-mode I+II (50–50%) |
|---|---|---|---|
| $x = 0$ | $u = 0, \quad v = 0$ | $v = 0, \quad w = 0$ | $v = 0$ |
| $x = 0.04$ | $u = 0, \quad v = 0$ | $v = 0, \quad w = 0$ | $v = 0$ |
| $y = 0$ | $v = 0$ | $v = 0, \quad w = 0$ | $v = 0$ |
| $y = 0.024$ | $v = 0$ | $v = 0, \quad w = 0$ | $v = 0$ |
| $z = 0$ | $w = 0$ | $u = -0.0005, \quad w = 0$ | $u = -0.00025, \quad w = 0$ |
| $z = 0.056$ | $w = 0.001$ | $u = \phantom{-}0.0005, \quad w = 0$ | $u = \phantom{-}0.00025, \quad w = 0.0005$ |

## 3. Results and Discussion

The distributions of the various stress components were investigated along the lines depicted in *Figs. 1* and *3* (line A–B, line C–D and line E–F). The line A–B represents the crack front, line C–D means the interface between the unidirectional layer and the insert film in the 2D model, and the fibre/matrix interface in the 3D model, respectively. The line E–F is also depicted in *Fig. 3* and was used to investigate the stress state ahead of the crack-tip.
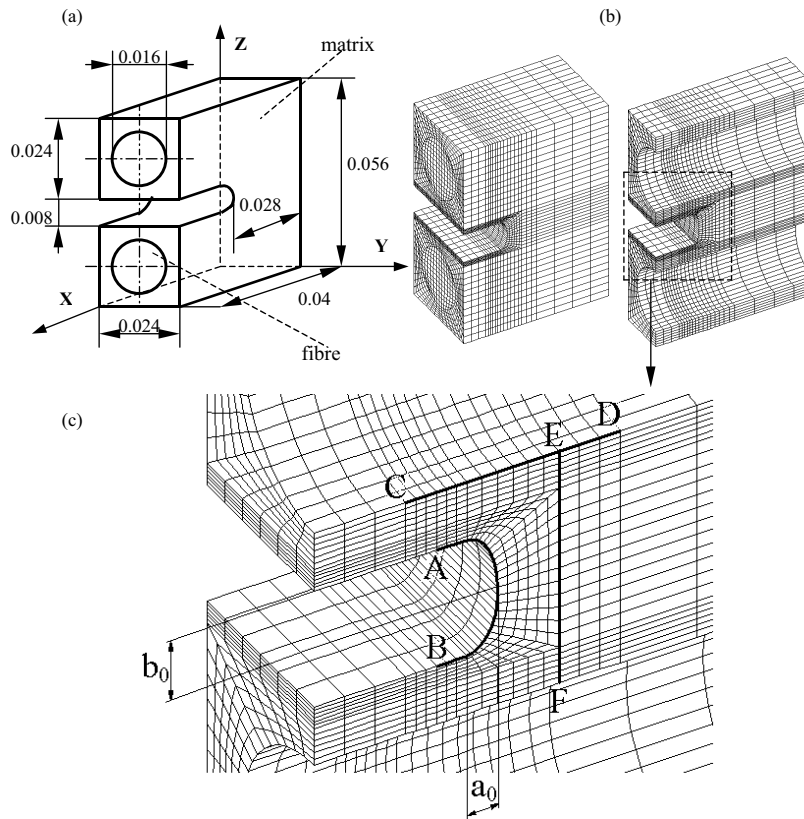
*Fig. 3.* Three-dimensional model (a), finite element mesh (b) and the details of the crack-tip (c). Line A–B – distance along the crack front, line C–D – distance along the fibre/matrix interface, line E–F – distance along the line ahead of the crack-tip (all distances in [mm]).

## 3.1. Results of the 2D Models

*Figs. 5—6* show the contour plot of the first principal ($\sigma_{p1}$) stress in the MMF and CLS specimens in the vicinity of the crack-tip. The lines show the transition in the stress pattern and concentration around the crack. The arrows in *Fig. 5* show the location of the point of maximum stress. Both specimens produce similar stress field, increasing the crack-tip bluntness the point of maximum stress moves from the tip towards the corner of the crack. The distribution of the principal stresses along the crack front is also illustrated in *Figs. 5–6* along line A–B (refer to *Fig. 1*). The results of *Figs. 5* and *6* show, that the crack bluntness decreases the values of $\sigma_{p1}$ in both the MMF and CLS specimens. A sharp starting crack increases
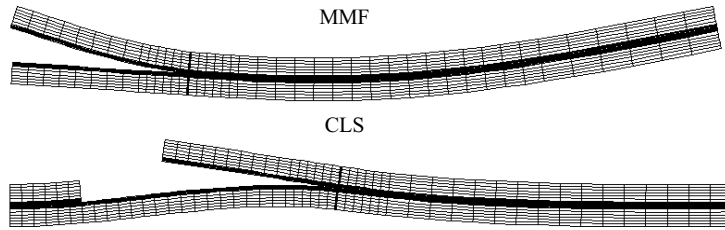
Fig. 4. Deformed shape of the 2D models (scale factor: 50)

the stress concentration in the corner of the crack. It should be noted that similar tendencies were obtained by TODO et al. for mode-I and mode-II loading conditions. Increasing the bluntness of the crack-tip the stress concentration decreases. The sharp crack exhibits a stress peak of 125 MPa in the MMF specimen and 215 MPa in the CLS specimen. Increasing the bluntness these peaks vanish. In the case of $a_0 = 0.004$ the first principal stress exhibits the value of 64 MPa in the MMF specimen and 106 MPa in the CLS specimen. TODO and co-workers reported 683 MPa in the case of $a_0 = 0.001$ and 321 MPa in the case of $a_0 = 0.004$ for the first principal stress according to the mode-I DCB tests [6]. The mode-II ENF tests produced similar values again by TODO et al. [7]. The differences between the current results and those produced by TODO et al. can be attributed to the different specimen configurations and loading conditions. It can be observed that the distribution in the CLS specimen shows the opposite trend as in the MMF specimen. This is due to the different loading conditions, and the fact that the CLS specimen deforms differently, as it is shown in *Fig. 4*. In *Fig. 7* the vector plot of the first principal stress shows that this component is tangential to the crack front where it reaches the maximum value. Hence the tensile failure of the matrix and crack growth towards the fibre/matrix interface is expected at this point, corresponding to the results in [6, 7].

### 3.2. Results of the 3D Analysis

#### 3.2.1. The Effect of Mode-I Contribution

As it is previously mentioned the mixed-mode condition was achieved by changing the percentage of the mode-I and mode-II displacement components. The mode-I contribution was varied from 0 to 100% including the pure mode-II (0% mode-I) and the pure mode-I loading conditions, respectively. The contour plot of the first principal stress and the distribution of the principal stresses along the crack front (line A–B) are illustrated in *Fig. 8* in the 3D model in the case of $a_0 = 0.002$. Again, the lines show the transition in the stress field. In pure mode-II the stress concentration occurs at the upper crack corner. Increasing the mode-I
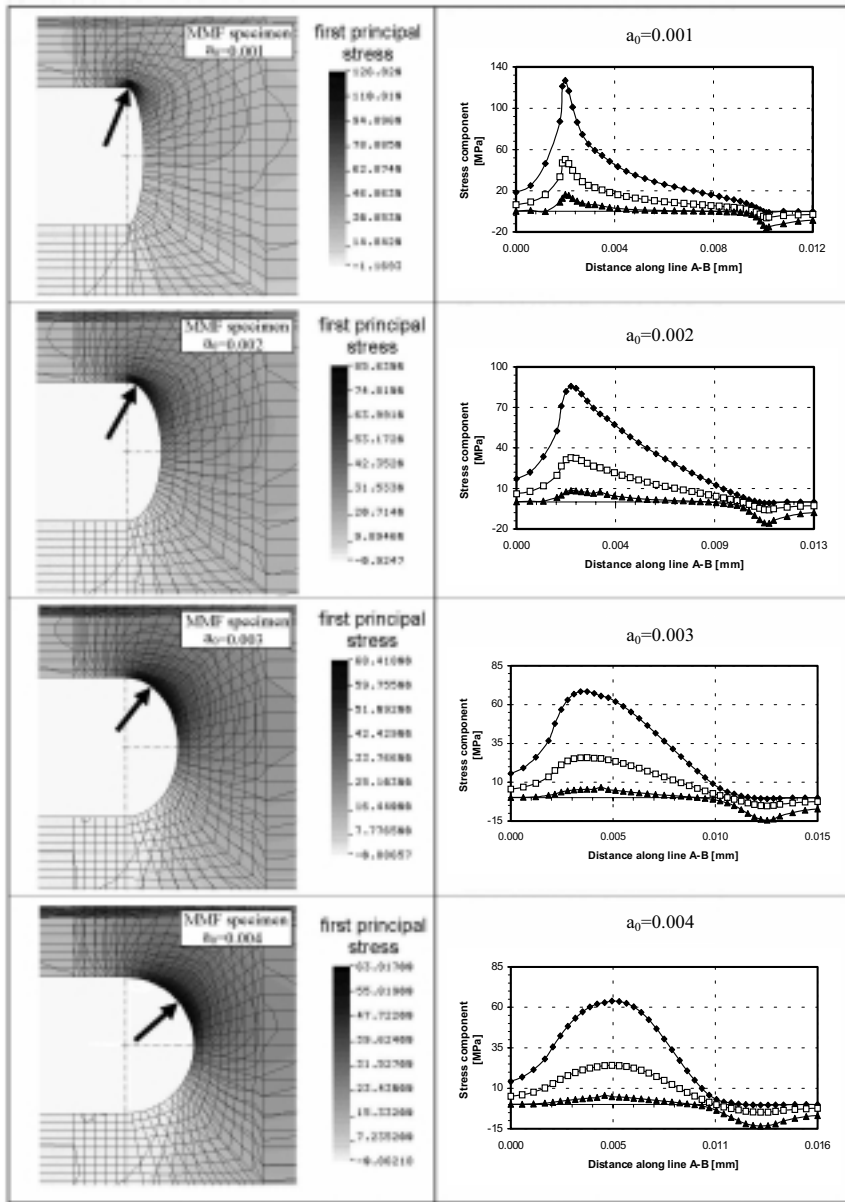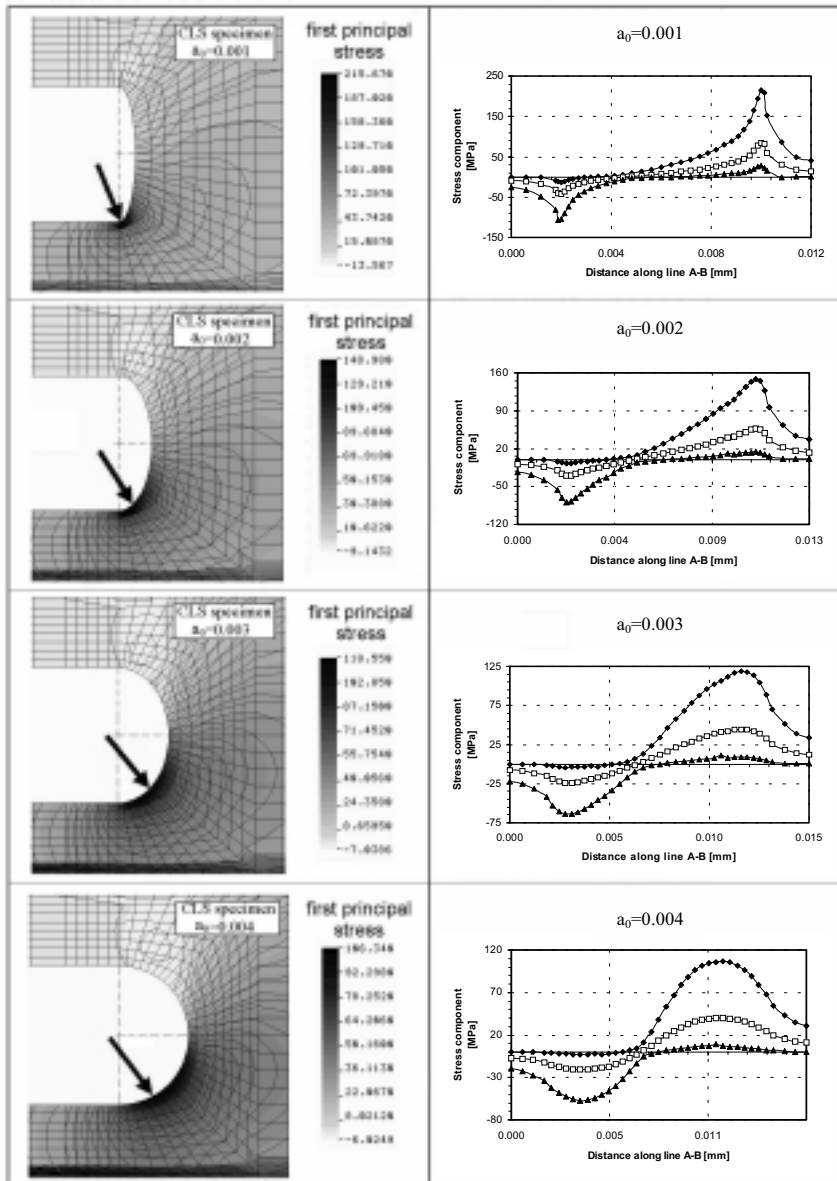
*Fig. 5*. Contour plot of the first principal stress around the crack-tip and distribution of the principal stresses along the crack front, MMF specimen, $\sigma_{p1}[\blacklozenge]$, $\sigma_{p2}[\square]$, $\sigma_{p3}[\blacktriangle]$

*Fig. 6.* Contour plot of the first principal stress around the crack-tip and distribution of the principal stresses along the crack front, CLS specimen, $\sigma_{p1}[\blacklozenge]$, $\sigma_{p2}[\square]$, $\sigma_{p3}[\blacktriangle]$
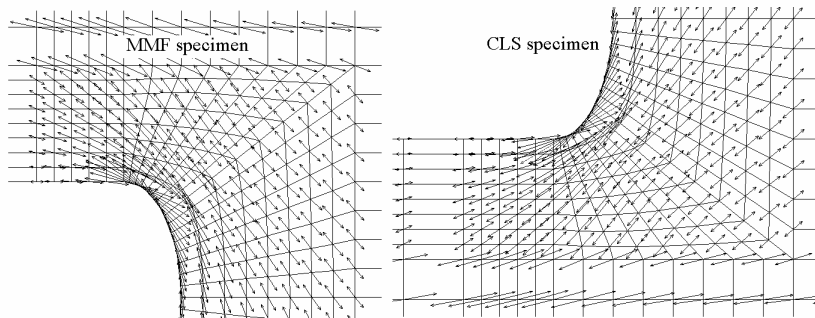
*Fig. 7.* Vector plot of the first principal stress directions in the 2D models

contribution the stress concentration can be observed at the upper and lower crack corners equally (symmetric distribution). The maximum of the first principal stress is about 174 MPa in 0% mode-I, 190 MPa in 20% mode-I, 220 MPa in 60% mode-I and about 295 MPa in 100% mode-I. In the latter case the extension of the stress concentration zone is much larger than in the former ones. *Fig. 9* illustrates the effects of mode-I contribution on the tensile stresses in the directions '*x*', '*z*' and the Von Mises equivalent stress around the crack-tip. The arrows show the maximum values in the actual stress pattern. Considering $\sigma_x$ the maximum occurs always in the corner of the crack, but in pure mode-I the maximum arises in both the upper and lower corners. The contour plot of $\sigma_z$ shows the maximum point moves from the crack corner towards the crack-tip increasing the mode-I contribution. The Von Mises stress shows similar trends. The tensile stresses along the fibre/matrix interface were investigated in the mid-plane of the 3D model as it is shown in *Fig. 10*. The effect of the mode-I contribution on the maximum of the first principal stress in the crack front and $\sigma_z$ in the fibre/matrix interface is illustrated in *Fig. 11*. It must be noted, that the point of maximum values changes its location increasing the mode-I contribution.

### 3.2.2. *The Crack Propagation Angle and the Critical Fibre/Matrix Interface Stress*

According to the stress distribution along the fibre/matrix interface there is a definite stress peak, which determines the crack progression path. On the other hand, in *Fig.7* it can be seen that in the point of maximal principal stress the stress is tangential to the crack front causing tensile failure of the matrix. It was assumed that the crack grows from the starting defect towards the fibre/matrix interface. This can be characterized by a crack angle, which can be determined by the location of the maximum of the first principal stress in the starting defect and the maximum of the tensile stress ($\sigma_z$) in the fibre/matrix interface. These points were connected with a curve according to *Fig. 12*. The crack angle was determined for mixed-mode I+II

conditions varying the mode-I contribution. The results of the analysis can be seen in *Fig. 13* (a). The crack angle shows very distinct values and no regularity can be found in *Fig. 13* (a). This can be attributed to that varying the mode-I contribution, both points of the crack growth path change its location. *Fig.13* (a) shows that the crack angle varies between $19°$ and $45°$ in mixed-mode loading conditions. From the 2D analysis the crack angle was found to be $29.9°$ in the MMF and $18.6°$ in the CLS specimens.

The critical values of the fibre/matrix interface stress were determined from the stress peaks. The peak value obtained from the distribution of the tensile stress $\sigma_z$ along the fibre/matrix interface was divided by the peak value obtained from the distribution of $\sigma_{p1}$ along the crack front. The results of the former computation are depicted in *Fig. 13* (b). In pure mode-II the critical percentage of the matrix stress is 22%, in pure mode-I it is 60%. Hence it can be concluded that in mode-II dominated loading in a relatively weak interface the crack rather grows towards the fibre/matrix interface, causing interfacial cracking and debonding than to grow along the mid-plane.

### 3.2.3. Tensile Stresses Ahead of the Crack-Tip

The tensile stresses ahead of the crack-tip were also investigated. *Fig. 14* shows the distribution of the tensile stresses ($\sigma_z$) ahead of the crack-tip (line E–F). Varying the mode-I contribution in all the cases the stress gradually decreases increasing the distance from the crack. The first chart shows the pure mode-II conditions (0% mode-I), the maximum stress value arises in the lower fibre/matrix interface. Similar effects can be seen in the 20% mode-I condition. As the mode-I contribution is significant the values of the stresses enhance and the maximum value arises near the interface. In pure mode-I loading the stress distribution reaches the maximum value at two points if the line E–F is far from the crack-tip. Close to the crack-tip the distribution contains three maximum points, including the middle of line E–F. We note, that the tensile stresses ahead of the-crack tip less distant than 0.006 mm from the crack-tip are slightly larger than the ones shown in *Fig. 14* but the current finite element mesh does not make possible to examine these stresses between the crack-tip and the point from 0.006 mm to it.

### 4. Conclusions

Two- and three-dimensional finite element analyses were carried out in order to investigate the stress concentration and crack initiation in mixed-mode I+II interlaminar fracture specimens. However, in fracture mechanics most of the models contain a crack, where the crack-tip is a singular point. The crack propagation is determined by the critical stress intensity factors, critical strain energy release rate, or other fracture criterion. This study is based on the research work of TODO
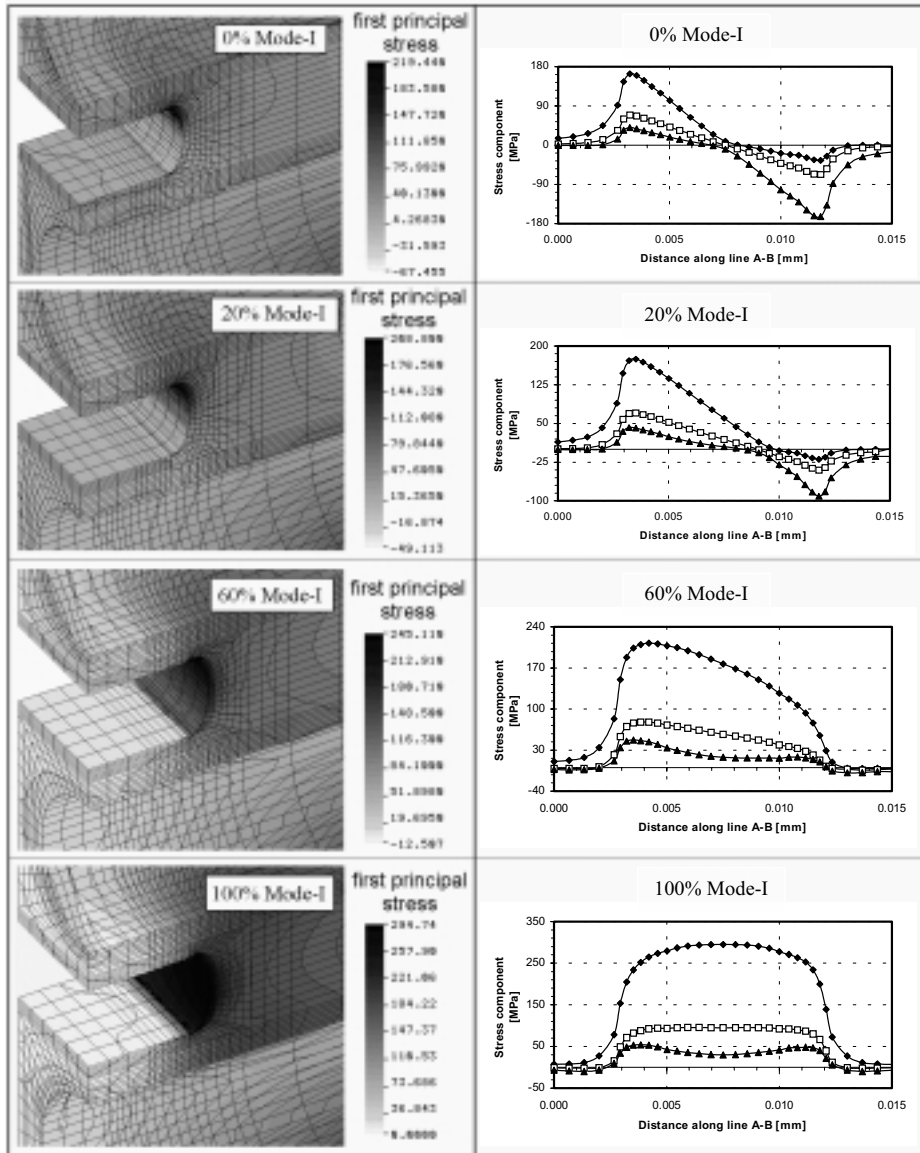
*Fig. 8.* Contour plot of the first principal stress around the crack-tip varying the mode-I contribution in the 3D model ($a_0 = 0.002$) and distribution of the principal stresses along the crack front, $\sigma_{p1}[\blacklozenge]$, $\sigma_{p2}[\square]$, $\sigma_{p3}[\blacktriangle]$
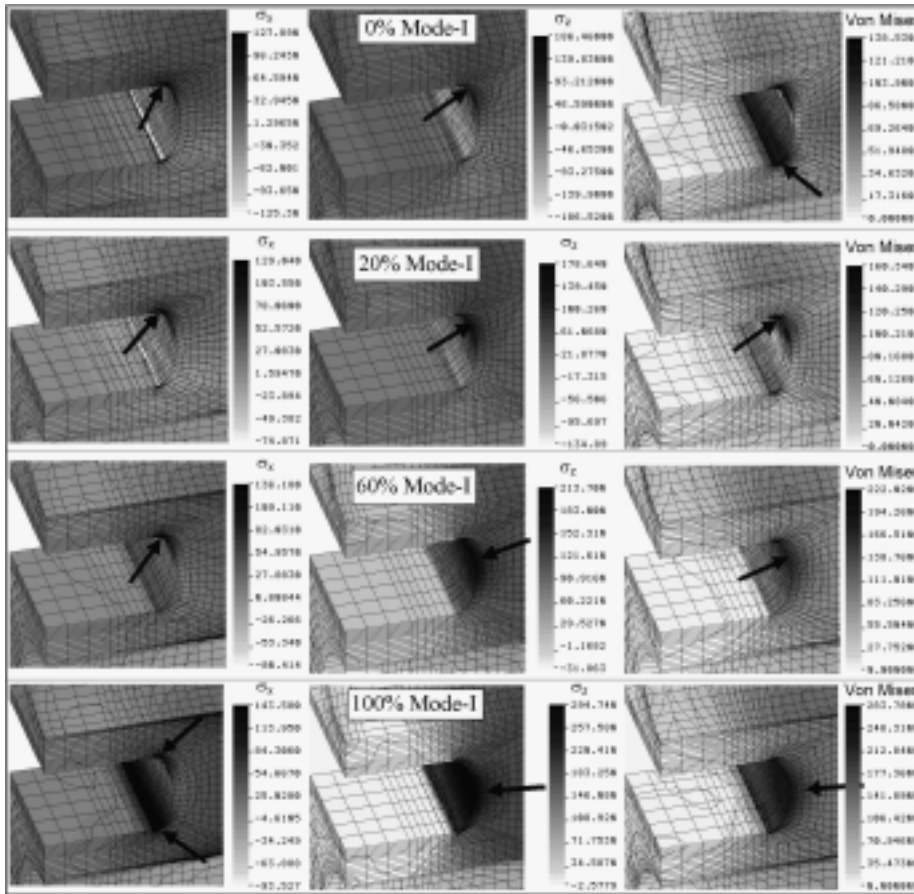
*Fig. 9.* Contour plot of the normal stresses in the *x*, *z* directions and the Von Mises equivalent stress. The arrows show the location of the maximum values of the actual stresses

and JAR [6, 7], who showed the elliptical shape of the crack front using scanning electron microscopy (SEM). However, the elliptical shape of the crack front is an idealization. According to this in the current study the singularity at the crack-tip was eliminated and analysis was carried out to find answer why the crack propagates along the fibre-matrix interface. Both the 2D and 3D models have a detailed crack-tip in order to investigate the stress concentration around the crack-tip. Two-dimensional models were used to represent the behavior of the composite MMF and CLS specimens. The mixed-mode I+II loading conditions in the three-dimensional model were achieved by prescribing the crack shearing and crack opening displacements for the boundary surfaces of the model. According to the results of the FE analysis the following conclusions can be drawn:
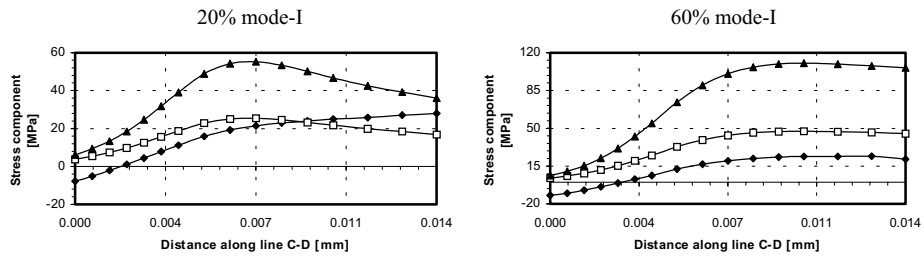
20% mode-I

60% mode-I



*Fig. 10.* Distribution of the Cartesian stresses along the fibre/matrix interface (line C–D). $\sigma_x[\blacklozenge]$, $\sigma_y[\square]$, $\sigma_z[\blacktriangle]$

(a)

(b)
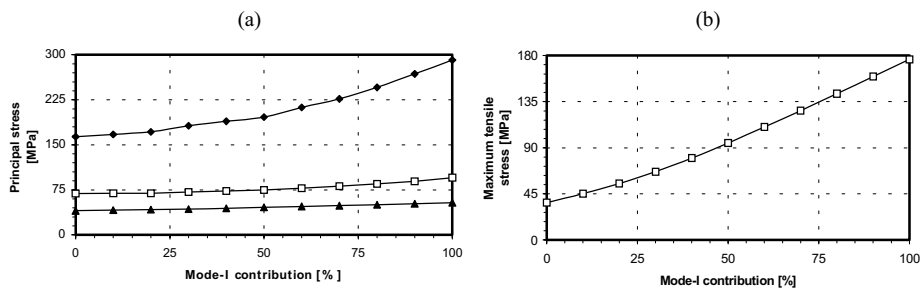


*Fig. 11.* The maximum of the principal stresses in the crack front as the function of mode-I contribution ($\sigma_{p1}[\blacklozenge]$, $\sigma_{p2}[\square]$, $\sigma_{p3}[\blacktriangle]$) (a). The maximum of the tensile stress $\sigma_z$ at the fibre/matrix interface as the function of mode-I contribution (b)
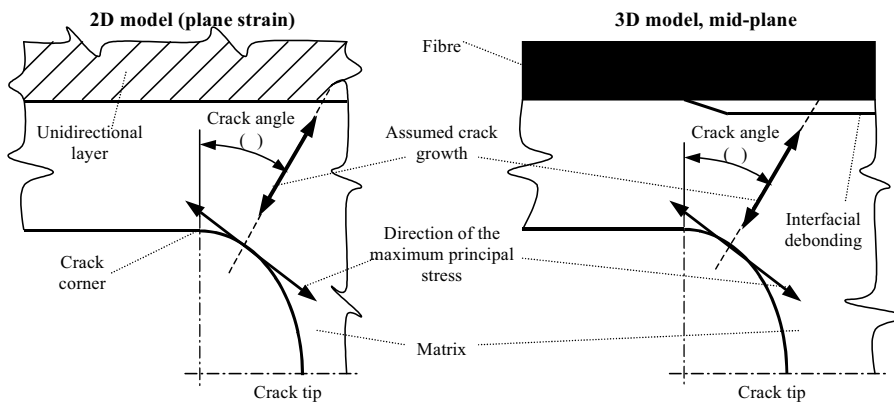


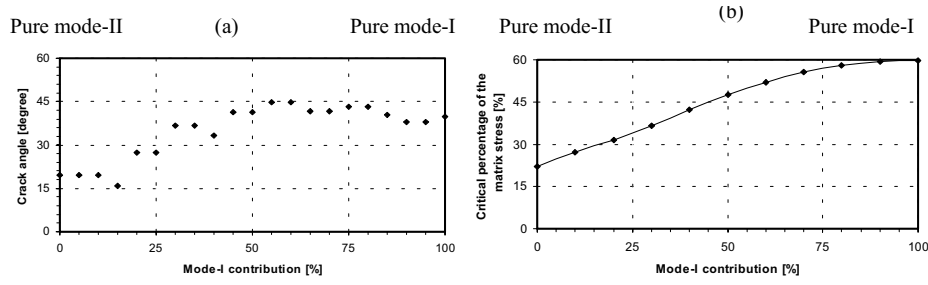*Fig. 12.* Assumed crack growth path and crack propagation angle

Pure mode-II     (a)     Pure mode-I     Pure mode-II     (b)     Pure mode-I



*Fig. 13*. Variation of the crack angle (a) and the critical interfacial stress (b) against the mode-I contribution



0% mode-I          20% mode-I

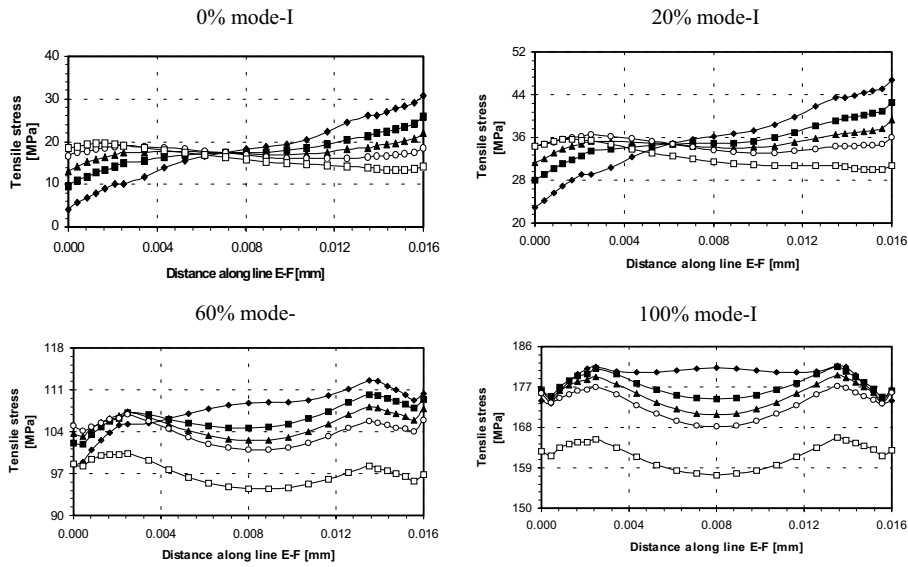60% mode-          100% mode-I

*Fig. 14*. Distribution of the tensile stresses ($\sigma_z$) ahead of the crack-tip. $x = 0.006$ ($\blacklozenge$), $x = 0.0073$ ($\blacksquare$), $x = 0.0087$ ($\blacktriangle$), $x = 0.01$ ($\circ$), $x = 0.015$ ($\square$). The numbers in parentheses are the distances between the tip and the line which is parallel to E–F (refer to *Fig. 3*)

- However, the values in the stress distribution are not too close to each other in the 2D and 3D models, similar tendencies were obtained.
- The maximum of the first principal stress was found to be always in the crack corner and tangential to the crack front in this point.
- The stress distribution was also observed in the unidirectional layer/insert film and the fibre/matrix interface, in both cases a clear stress peak arises

causing the crack to grow towards the fibre/matrix interface.

- The crack propagation angle was determined and found to be increasing with the mode-I contribution of 55%, and slightly decreasing above this value.
- The critical interface stress was determined by changing the mode-I contribution from 0% to 100%, the critical interface stress increases with the mode-I contribution indicating that in mode-II dominated loading the interfacial crack can arise prior to interlaminar crack propagation in the insert film.
- The tensile stresses ahead of the crack-tip show that the location and the value of the maximum stress varies with the mode-I contribution, in pure mode-II the maximum point arises at the lower fibre/matrix interface, while in mode-I the distribution has larger values and three maximum points (including the middle of line E–F) can be observed.

## Acknowledgements

## References

[1] KUSAKA, T. – HOJO, M. – MAY, Y. W. – KUROKAWA, T. – NOJIMA, T. – OCHIAI, S., Rate Dependence of Mode I Fracture Behaviour in Carbon-Fibre/Epoxy Composite Laminates, *Composites Science and Technology*, **58** (1998), pp. 591–602.

[2] COMPSTON, P. – JAR, P. Y. B. – BURCHILL, P. J. – TAKAHASHI, K., The Effect of Matrix Toughness and Loading Rate on the Mode-II Interlaminar Fracture Toughness of Glass-Fibre/Vinyl-Ester Composites, *Composites Science and Technology*, **61** (2001), pp. 321–333.

[3] KENANE, M. – BENZEGGAGH, M. L., Mixed-Mode Delamination Fracture Toughness of Unidirectional Glass/Epoxy Composites under Fatigue Loading, *Composites Science and Technology*, **57** (1997), pp. 597–605.

[4] ALLIX, O. – LÉVÉQUE, D. – PERRET, L., Identification and Forecast of Delamination in Composite Laminates by an Interface Model, *Composites Science and Technology*.

[5] REYES, G. – CANTWELL, W. J., The Mechanical Properties of Fibre-Metal Laminates Based on Glass Fibre Reinforced Polypropylene, *Composites Science and Technology*, **60** (2000), pp. 1085–1094.

[6] TODO, M. – JAR, P. Y. B., Study of Mode-I Interlaminar Crack Growth in DCB Specimens of Fibre-Reinforced Composites, *Composites Science and Technology*, **58** (1998), pp. 105–118.

[7] TODO, M. – JAR, P. Y. B. – TAKAHASHI, K., Initiation of a Mode-II Interlaminar Crack from an Insert Film in End-Notched Flexure Composite Specimen, *Composites Science and Technology*, **60** (2000), pp. 263–272.